

# Solid State Coordination Chemistry in the Design of Molybdenum Oxides: The Hydrothermal Synthesis and Structure of a Layered Copper–Molybdenum Oxide, $[\text{Cu}(\text{tpytrz})_2\text{Mo}_4\text{O}_{13}]$ (tpytrz = tripyridyltriazine)

Douglas E. Hagrman and Jon Zubieta<sup>1</sup>

Department of Chemistry, Syracuse University, Syracuse, New York 13244-4100, and W. M. Keck Center for Molecular Electronics, Syracuse University, Syracuse, New York 13244-4100

The hydrothermal reaction of  $\text{CuSO}_4 \cdot 5\text{H}_2\text{O}$ , tripyridyltriazine (tpytrz),  $\text{MoO}_3$ , and  $\text{H}_2\text{O}$  in the mole ratio 2.1:1.0:1.9:3470 for 84 h at 160°C yields green needles of  $[\text{Cu}(\text{tpytrz})_2\text{Mo}_4\text{O}_{13}]$  (MOXI-37). The structure of MOXI-37 consists of bimetallic  $\{\text{CuMo}_4\text{O}_{13}\}$  layers buttressed by tpytrz ligands occupying the interlamellar region. The overall structure adopts the motif of alternating inorganic and organic subunits characteristic of many organic–inorganic composite materials. The inorganic network is constructed from  $\{\text{Mo}_4\text{O}_{13}\}$  chains of corner-sharing octahedra and tetrahedra, linked by octahedral  $\{\text{CuN}_2\text{O}\}$  units into a two-dimensional structure. The structure of MOXI-37 may be compared to other examples of copper–molybdate networks sandwiching bridging organonitrogen ligands, namely,  $[\text{Cu}(\text{dpe})\text{MoO}_4]$  (MOXI-1) and  $[\text{Cu}(\text{bpa})_{0.5}\text{MoO}_4]$  (MOXI-24). In contrast to the network connectivity of MOXI-37, the layer structure of  $[\text{Cu}(\text{dpe})\text{MoO}_4]$  consists of corner-sharing  $\{\text{MoO}_4\}$  tetrahedra and  $\{\text{CuN}_2\text{O}_5\}$  trigonal bipyramids, while the two-dimensional oxide substructure  $[\text{Cu}(\text{bpa})_{0.5}\text{MoO}_4]$  is constructed from tetranuclear copper clusters linked through corner-sharing  $\{\text{MoO}_4\}$  tetrahedra. © 2000 Academic Press

The oxides are ubiquitous materials whose vast range of properties derives from their diversity of chemical composition and structure types (1, 2). However, while many naturally occurring oxides and minerals possess complex crystal structures, the majority are of simple composition and have highly symmetrical structures with rather small unit cells. Most silicates, important ores, gems, many rocks, and soils are examples of these materials. Although such simple oxides can possess unique and specific properties, such as piezoelectricity, ferromagnetism, and catalytic activity, as a general rule there is a correlation between the

complexity of the structure of a material and its functionality.

One approach to the design of oxide materials exploits organic components to modify the inorganic microstructure. The most extensively studied manifestations of such organic–inorganic composite materials are zeolites (3), MCM-41 mesoporous materials (4), and transition metal phosphates (5) where the organic constituent is present as a charge-compensating, space-filling and structure-directing subunit, as shown schematically in Fig. 1a. An alternative approach relies on the principles of fundamental coordination chemistry to modify the oxide microstructure. In this instance, the organic component is introduced as a ligand to a secondary metal site, which functions as an integral subunit of the covalent architecture of the solid. Consequently, the overall structure reflects the coordination preferences of the secondary metal site, which are reflected in polyhedral type adopted, donor group attachments and degree of aggregation into oligomeric units, and the geometric constraints of the ligand. The emphasis lies in the design of the ligands and the coordination preferences of the secondary metal site to provide defined structural subunits for fashioning the oxide structure. The secondary metal centers provide not only distinct geometric biases but a range of binding strengths to the oxide skeleton, of formation kinetics, and of photochemical, electrochemical, magnetic, and reaction properties.

The approach we have adopted conflates oxide chemistry and the emerging field of crystal engineering of coordination polymers (6, 7). In designing coordination polymers, the expectation is that the structural information inherent in the metal coordination preferences will be propagated through the bridging ligands. The method for preparing such coordination polymers has exploited organic ligands which through their geometries and coordination preferences impose a specific topology: chain (1D), ladder (1D), brick

<sup>1</sup> To whom correspondence should be addressed.



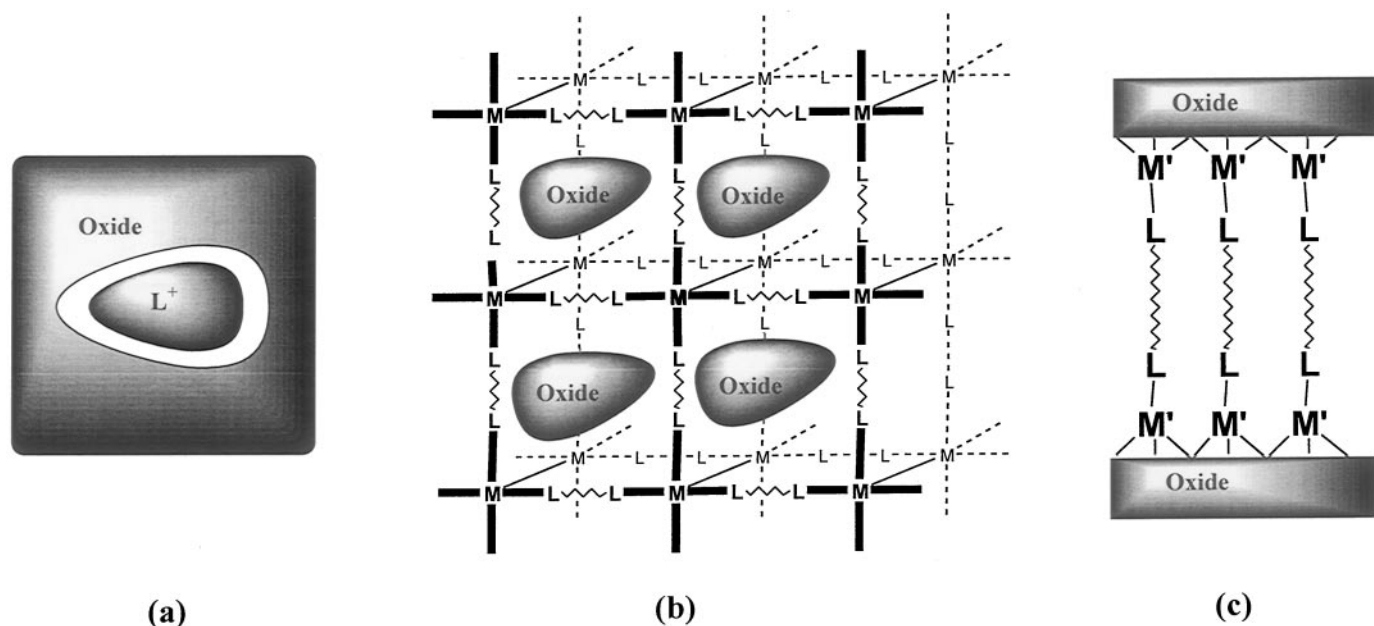


**FIG. 1.** (a) Schematic representation of the entrapment of a charge-compensating, space-filling, and structure directing organic cation within an oxide framework. (b) An oxide substructure confined within the scaffolding of a coordination complex polymer cation. (c) Schematic view of the incorporation of a secondary metal site into the oxide substructure. The ligand serves to “buttress” the bimetallic oxide networks.

network (2D), bilayer (2D), and framework (3D). From the specific perspective of the structural modification of molybdenum oxide phases, the secondary metal–organonitrogen polymer subunits may be regarded as cationic moieties which provide not only charge compensation and space-filling requirements but also a scaffolding of variable charge, topology, and channel dimensions for the incorporation of oxide subunits. In the naïve representation of Fig. 1b, the structure of the oxide component will conform to the constraints of the cationic skeleton.

This approach has proved fruitful in the preparation of a variety of molybdenum oxides such as  $[\{\text{Cu}(4,4'\text{-bpy})\}_4\text{Mo}_8\text{O}_{26}]$  (**MOXI-12**),  $[\{\text{Ni}(4,4'\text{-bpy})\}_2(\text{H}_2\text{O})_2\}_2\text{Mo}_8\text{O}_{26}]$  (**MOXI-14**),  $[\{\text{Cu}(4,4'\text{-bpy})\}_4\text{Mo}_{15}\text{O}_{47}]$  (**MOXI-16**), and  $[\{\text{Cu}(\text{bpe})\}_4\text{Mo}_8\text{O}_{26}]$  (**MOXI-13**) (8, 9). In these structures, the molybdenum oxide and the secondary metal–organonitrogen complex are present as distinct anionic and cationic substructures, respectively, an observation which reflects the pronounced proclivity of Cu(I) to adopt a diagonal coordination mode with pyridyl donor ligands. However, an alternative structural type emerges upon modification of the ligand geometry and the secondary metal site and its coordination preferences. In this class of materials, the secondary metal site is directly incorporated into the oxide substructure to produce a bimetallic oxide material, as shown schematically in Fig. 1c. Two examples of such composites have been reported recently by us, namely, the layered phases  $[\text{Cu}(\text{dpe})(\text{MoO}_4)]$  (**MOXI-1**) (10) and  $[\text{Cu}(\text{bpa})_{0.5}\text{MoO}_4]$  (**MOXI-24**) (11). In these latter mater-

ials, the preference of Cu(II) for expanded coordination numbers of five or six (4 + 1 or 4 + 2 axially distorted geometries), in contrast to Cu(I), and the enhanced oxophilicity of Cu(II) with respect to Cu(I) has been exploited in the design of the bimetallic oxide networks. In

**TABLE 1**  
**Summary of Crystallographic Data for  $[\text{Cu}(\text{tpytrz})_2\text{Mo}_4\text{O}_{13}]$  (**MOXI-37**)**

Empirical formula	$\text{C}_{18}\text{H}_{12}\text{N}_6\text{O}_{6.5}\text{Cu}_{0.5}\text{Mo}_2$
fw	639.98
Crystal system	Triclinic
Space group	<i>P</i> -1
<i>a</i> (Å)	8.1011(2)
<i>b</i> (Å)	9.1551(2)
<i>c</i> (Å)	13.6071(3)
$\alpha$ (°)	79.200(1)
$\beta$ (°)	83.589(1)
$\gamma$ (°)	78.661(1)
Volume (Å <sup>3</sup> )	969.03(4)
<i>Z</i>	2
$D_{\text{calc}}$ (g cm <sup>-3</sup> )	2.194
$\mu(\text{MoK}\alpha)$ (cm <sup>-1</sup> )	18.84
<i>R</i> 1	0.0504
<i>wR</i> 2	0.1597
$R1 = \sum(F_o - F_c)/\sum(F_o)$	
$wR2 = [\sum[w(F_o^2 - F_c^2)^2]/\sum w(F_o^2)^2]^{1/2}$	

**TABLE 2**  
Atomic Coordinates ( $\times 10^4$ ) and Equivalent Isotropic Displacement Parameter ( $\text{\AA}^2 \times 10^3$ ) for  $[\text{Cu}(\text{tpytrz})_2\text{Mo}_4\text{O}_{13}]$

	x	y	z	U(eq)
Mo(1)	1988(1)	3837(1)	4480(1)	4(1)
Mo(2)	-3365(1)	3181(1)	4244(1)	5(1)
Cu(1)	0	0	5000	5(1)
O(1)	1918(6)	4699(6)	3261(4)	10(1)
O(2)	0	5000	5000	7(2)
O(3)	4446(6)	2945(6)	4317(4)	8(1)
O(4)	1242(6)	2189(6)	4504(4)	8(1)
O(5)	-2124(6)	1397(6)	4629(4)	8(1)
O(6)	-3103(6)	4476(6)	5020(4)	8(1)
O(7)	-2689(7)	3826(7)	3030(4)	12(1)
N(1)	9011(8)	-6409(8)	-122(6)	13(2)
N(2)	2613(7)	2523(8)	-3811(5)	7(1)
N(3)	605(7)	-291(7)	3549(5)	4(1)
N(4)	4770(7)	-1602(7)	-1028(5)	7(1)
N(5)	2660(7)	-7(7)	-161(5)	7(1)
N(6)	4240(7)	-2259(7)	732(5)	6(1)
C(1)	8585(9)	-5464(9)	-990(6)	8(2)
C(2)	7331(9)	-4191(9)	-1026(6)	7(2)
C(3)	6443(9)	-3845(9)	-132(6)	7(2)
C(4)	6844(9)	-4806(9)	769(6)	9(2)
C(5)	8133(9)	-6083(9)	723(6)	7(2)
C(6)	1885(9)	2957(9)	-2943(6)	8(2)
C(7)	2132(9)	2027(9)	-1994(6)	8(2)
C(8)	3210(8)	639(9)	-1957(6)	5(2)
C(9)	3963(9)	193(9)	-2859(6)	10(2)
C(10)	3632(10)	1151(10)	-3760(7)	14(2)
C(11)	1388(9)	-1688(9)	3378(6)	9(2)
C(12)	2196(9)	-1952(9)	2461(6)	8(2)
C(13)	2117(9)	-739(9)	1650(6)	8(2)
C(14)	1206(9)	674(9)	1788(6)	7(2)
C(15)	502(9)	881(10)	2756(6)	11(2)
C(16)	5082(8)	-2510(9)	-148(6)	5(2)
C(17)	3570(9)	-383(9)	-989(6)	8(2)
C(18)	3047(9)	-1000(9)	687(6)	7(2)

extending the chemistry of this class of composite oxides, the role of more sterically demanding ligands in sculpting the interlamellar volume has been investigated. As part of these studies, the potentially tridentate tripyridyltriazine (tpytrz) ligand has been incorporated into copper(II) molybdate phases. The compound  $[\text{Cu}(\text{tpytrz})_2\text{Mo}_4\text{O}_{13}]$  (**MOXI-37**) exhibits copper molybdate two-dimensional networks of unique  $\{\text{CuMo}_4\text{O}_{13}\}$  composition and structure, buttressed by bridging, bidentate tripyridyltriazine ligands.

## EXPERIMENTAL

*General considerations.* All reagents were purchased from Aldrich Chemicals and used without further purification.

Reactions were carried out in polytetrafluoroethylene-lined stainless steel containers under autogenous pressure. The 23-ml reaction vessels were filled to approximately 40% volume capacity.

X-ray diffraction studies were performed on a Bruker SMART System equipped with a CCD detector, using  $\text{MoK}\alpha$  radiation ( $\lambda = 0.71073 \text{ \AA}$ ) at 100 K (12). Data were corrected for Lorentz and polarization effects, and absorption corrections were made using SADABS (13). The structure solution and refinement were carried out using the SHELXL96 software package (14). The structure was solved by direct methods. After locating all of the nonhydrogen

**TABLE 3**  
Selected Bond Lengths ( $\text{\AA}$ ) and Angles ( $^\circ$ ) for  $[\text{Cu}(\text{tpytrz})_2\text{Mo}_4\text{O}_{13}]$

Mo(1)–O(1)	1.701(6)	O(1)–Mo(1)–O(4)	103.8(3)
Mo(1)–O(4)	1.726(6)	O(1)–Mo(1)–O(2)	97.78(17)
Mo(1)–O(2)	1.8924(6)	O(4)–Mo(1)–O(2)	98.90(17)
Mo(1)–O(3)	2.003(5)	O(1)–Mo(1)–O(3)	93.7(2)
Mo(1)–O(6) <sup>a</sup>	2.178(6)	O(4)–Mo(1)–O(3)	96.5(2)
Mo(1)–N(2) <sup>b</sup>	2.467(7)	O(2)–Mo(1)–O(3)	157.98(18)
Mo(2)–O(7)	1.713(6)	O(1)–Mo(1)–O(6) <sup>a</sup>	96.0(3)
Mo(2)–O(5)	1.762(5)	O(4)–Mo(1)–O(6) <sup>a</sup>	160.0(3)
Mo(2)–O(6)	1.785(6)	O(2)–Mo(1)–O(6) <sup>a</sup>	80.79(13)
Mo(2)–O(3) <sup>c</sup>	1.818(5)	O(3)–Mo(1)–O(6) <sup>a</sup>	79.4(2)
Cu(1)–O(5)	1.985(5)	O(1)–Mo(1)–N(2) <sup>b</sup>	170.3(2)
Cu(1)–O(5) <sup>d</sup>	1.985(5)	O(4)–Mo(1)–N(2) <sup>b</sup>	79.8(2)
Cu(1)–N(3) <sup>d</sup>	2.035(7)	O(2)–Mo(1)–N(2) <sup>b</sup>	90.48(14)
Cu(1)–N(3)	2.035(7)	O(3)–Mo(1)–N(2) <sup>b</sup>	76.9(2)
Cu(1)–O(4)	2.370(5)	O(6) <sup>a</sup> –Mo(1)–N(2) <sup>b</sup>	80.2(2)
Cu(1)–O(4) <sup>d</sup>	2.370(5)	O(7)–Mo(2)–O(5)	107.9(3)
		O(7)–Mo(2)–O(6)	109.1(3)
		O(5)–Mo(2)–O(6)	110.1(3)
		O(7)–Mo(2)–O(3) <sup>c</sup>	110.3(3)
		O(5)–Mo(2)–O(3) <sup>c</sup>	108.1(2)
		O(6)–Mo(2)–O(3) <sup>c</sup>	111.3(2)
		O(5)–Cu(1)–O(5) <sup>d</sup>	180.0(3)
		O(5)–Cu(1)–N(3) <sup>d</sup>	89.0(2)
		O(5)–Cu(1)–N(3)	91.0(2)
		O(5) <sup>d</sup> –Cu(1)–N(3)	89.0(2)
		N(3) <sup>d</sup> –Cu(1)–N(3)	180.0
		O(5)–Cu(1)–O(4)	84.28(19)
		O(5) <sup>d</sup> –Cu(1)–O(4)	95.72(19)
		N(3) <sup>d</sup> –Cu(1)–O(4)	95.6(2)
		N(3)–Cu(1)–O(4)	84.4(2)
		O(4)–Cu(1)–O(4) <sup>d</sup>	180.0
		Mo(1)–O(2)–Mo(1) <sup>a</sup>	180.000(1)
		Mo(2) <sup>e</sup> –O(3)–Mo(1)	148.9(3)
		Mo(1)–O(4)–Cu(1)	164.3(3)
		Mo(2)–O(5)–Cu(1)	154.4(3)
		Mo(2)–O(6)–Mo(1) <sup>a</sup>	157.7(3)

*Note.* Symmetry transformations used to generate equivalent atoms: <sup>a</sup>  $-x, -y + 1, -z + 1$ . <sup>b</sup>  $x, y, z + 1$ . <sup>c</sup>  $x - 1, y, z$ . <sup>d</sup>  $-x, -y, -z + 1$ . <sup>e</sup>  $x + 1, y, z$ .

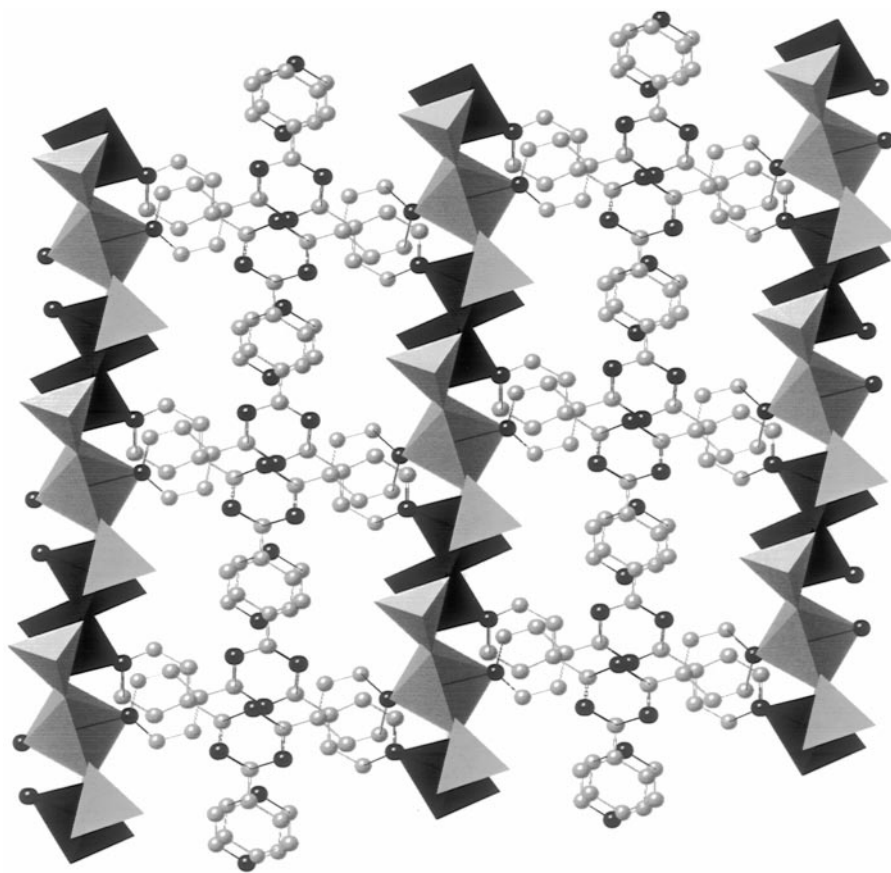


FIG. 2. A view of the layered structure of  $[\text{Cu}(\text{tpytrz})_2\text{Mo}_4\text{O}_{13}]$  (MOXI-37) parallel to the crystallographic  $a$  axis.

atoms, the model was refined against  $F^2$ , initially using isotropic, and later anisotropic, thermal parameters until the final value of  $\Delta/\sigma_{\text{max}}$  was less than 0.001. At this point, the hydrogen atoms were placed in idealized positions and the final cycle of refinements was performed.

**Synthesis of  $[\text{Cu}(\text{tpytrz})_2\text{Mo}_4\text{O}_{13}]$  (MOXI-37).** A solution of tripyridyltriazine (0.050 g, 0.16 mmol),  $\text{MoO}_3$  (0.044 g, 0.31 mmol),  $\text{CuSO}_4 \cdot 5\text{H}_2\text{O}$  (0.082 g, 0.35 mmol), and  $\text{H}_2\text{O}$  (10 g, 555.6 mmol) in the mole ratio 1.0:1.9:2.1:3470 was heated at  $160^\circ\text{C}$  for 84 h. After cooling, green crystals were obtained as a monophasic product in 70% yield. IR (KBr pellet,  $\text{cm}^{-1}$ ): 1620(m), 1575(m), 1463(m), 1408(s), 1220(m), 1100(m), 925(s), 890(s), 840(m), 790(s), 640(m).

## RESULTS AND DISCUSSION

The bimetallic oxide MOXI-37 was prepared in the hydrothermal reaction of  $\text{CuSO}_4 \cdot 5\text{H}_2\text{O}$ ,  $\text{MoO}_3$ , and tripyridyltriazine. While MOXI-37 can be isolated in low yield over a range of reactant stoichiometries, the values reported are necessary for optimization. Furthermore, the temperature and pH are crucial in maintaining the Cu(II)

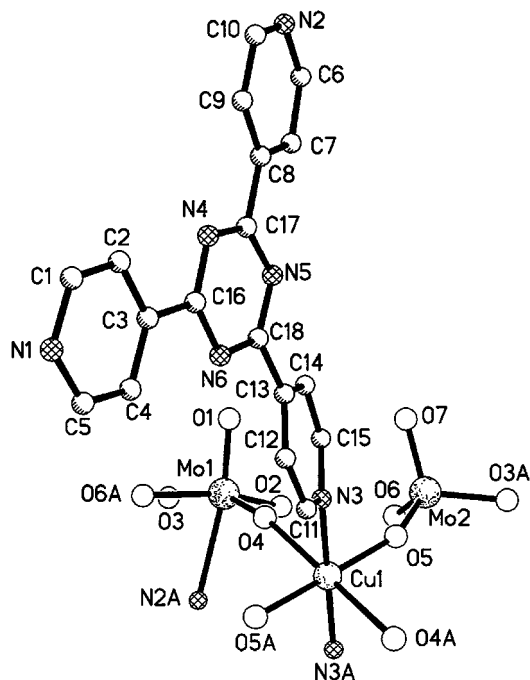
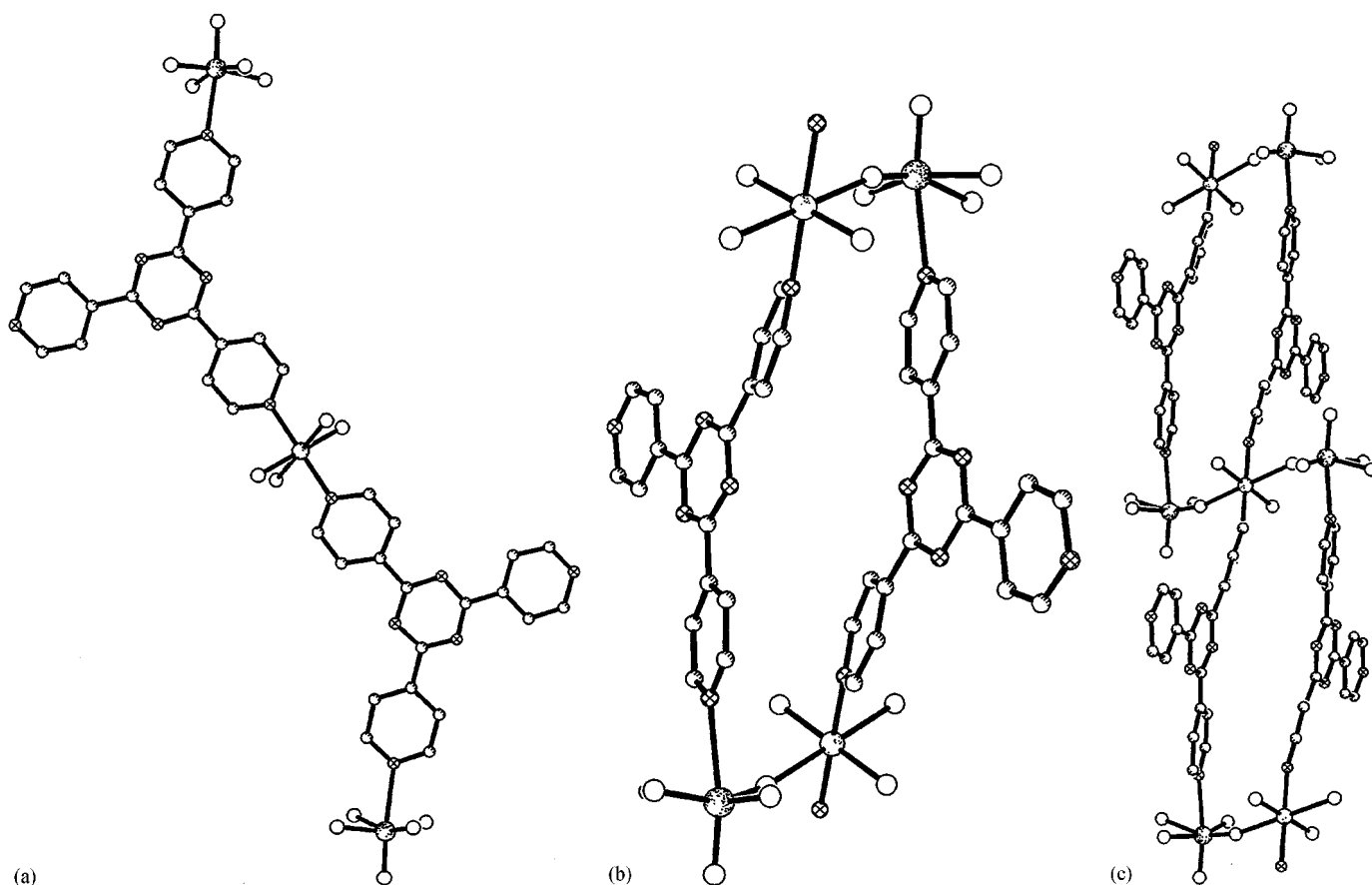


FIG. 3. A view of the copper-ligand geometry and of the molybdenum coordination geometries of MOXI-37, showing the atom-labeling scheme.



**FIG. 4.** (a) The copper-bistripyridyltriazine subunit of **MOXI-37**, participating in linking three inorganic layers. (b) The  $\{\text{Cu}_2\text{Mo}_2\text{O}_2(\text{tpytrz})_2\}$  ring structure linking two adjacent layers of **MOXI-37**. (c) The offset between neighboring  $\{\text{Cu}_2\text{Mo}_2\text{O}_2(\text{tpytrz})_2\}$  rings of **MOXI-37**.

oxidation state and avoiding the precipitation of mixtures of Cu(I)-containing phases.

As shown in Fig. 2, the overall structure of **MOXI-37** consists of layers of corner-sharing Cu(II) octahedra and Mo(VI) octahedra and tetrahedra, buttressed by tpytrz ligands occupying the interlamellar region. The structure is reminiscent of the oxovanadium organophosphonate family (15) which also exhibits inorganic metal oxide networks with organic scaffolding between the layers.

As shown in Fig. 3, the individual building blocks consist of an octahedral Cu(II) site with  $\{\text{CuN}_2\text{O}_4\}$  coordination geometry defined by nitrogen donors from each of two tpytrz ligands occupying *trans* coordination sites and four oxo-groups from four adjacent molybdate polyhedra; a tetrahedral  $\{\text{MoO}_4\}$  site with three oxo-groups participating in bridging to two adjacent molybdenum sites and one copper site and with one terminal oxo-group; and an octahedral  $\{\text{MoNO}_3\}$  center whose geometry is defined by a nitrogen donor from a tpytrz ligand, four oxo-groups which bridge to three molybdenum and one copper sites, and a terminal oxo-group.

The tripyridyltriazine ligand exhibits two unusual features. One arm of the ligand is pendant and, rather than ligating to a metal site, participates in  $\pi$ -stacking in the interlamellar region. Furthermore, each ligand coordinates to a copper site and to a molybdenum site. As discussed below, this feature contrasts with the structures of **MOXI-1** and **MOXI-24**, where the nitrogen donors are exclusively ligated to copper sites. In fact, in all other examples of molybdenum oxide–secondary metal–ligand phases, the nitrogen donors are associated with the secondary metal site rather than the molybdenum centers.

The structural consequences of this ligation mode are evident in Fig. 4. The *trans* disposition of the tpytrz ligands about the Cu sites, together with their bidentate coordination mode, results in the motif of Fig. 4a, in which each  $\{\text{Cu}(\text{tpytrz})_2\}$  subunit participates in the construction of three layers: the oxide layer containing the Cu site and the layers above and below, which are linked through the tpytrz ligands bridging to Mo centers. The unusual coordination mode of the ligands generates the unique structural motif of Fig. 4b, a heterocyclic structure containing two ligands and

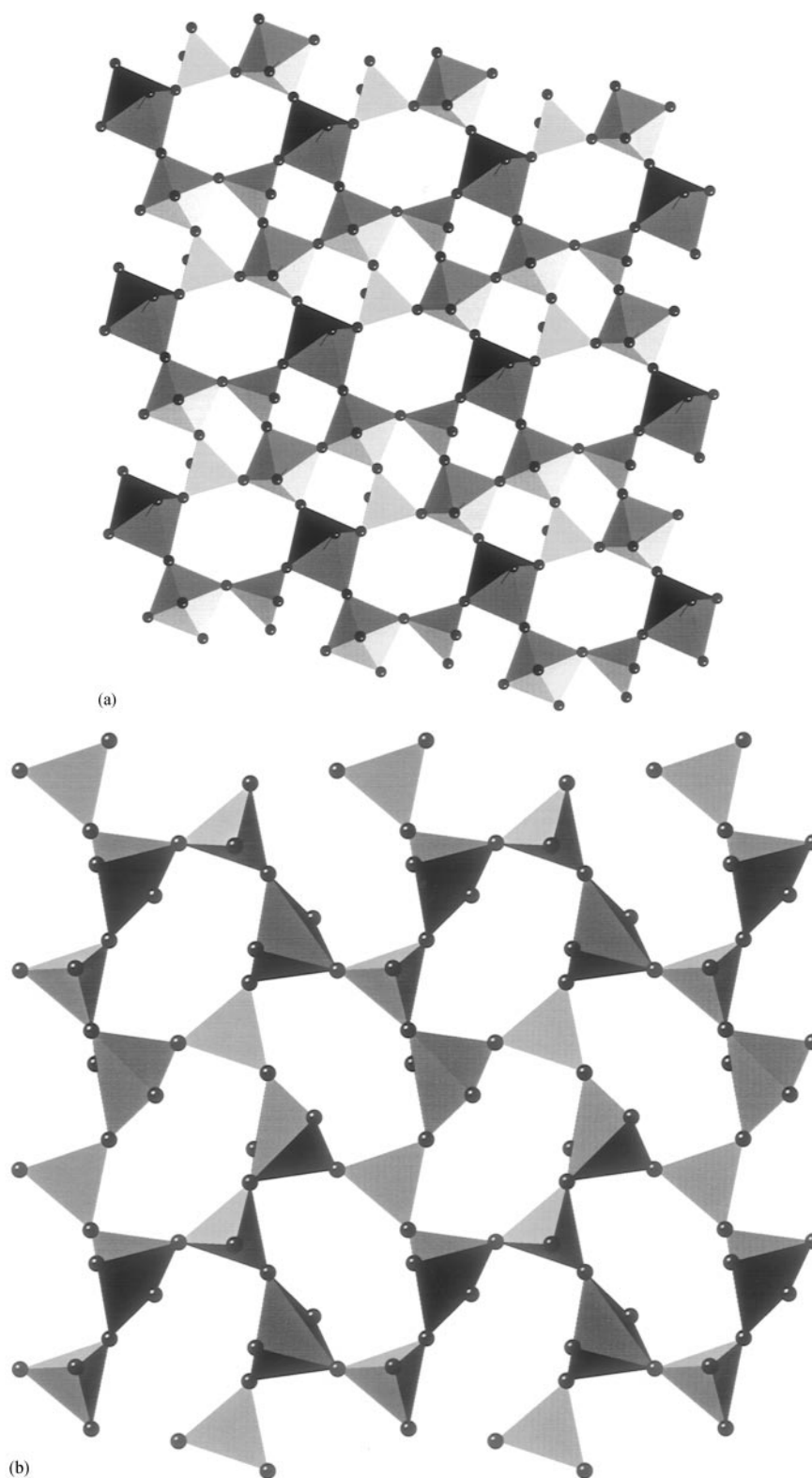


**FIG. 5.** (a) The  $\{\text{CuMo}_4\text{O}_{13}\}$  layer of **MOXI-37**, viewed parallel to the  $c$  axis. The dark octahedra represent the copper sites, while the lighter octahedra and tetrahedra are the molybdenum sites. (b) The  $\{\text{CuMoO}_4\}$  layer of  $[\text{Cu}(\text{dpe})\text{MoO}_4]$  (**MOXI-1**). The tetrahedra are the Mo sites, while the trigonal bipyramids represent the copper centers. (c) The  $\{\text{CuMoO}_4\}$  layer of  $[\text{Cu}(\text{bpa})_{0.5}\text{MoO}_4]$  (**MOXI-24**). The molybdenum sites are represented by tetrahedra, and the copper sites by the octahedrally coordinated gray spheres. The interlamellar spacings for **MOXI-37**, **MOXI-1**, and **MOXI-24** are 13.6, 11.2, and 13.7 Å, respectively.

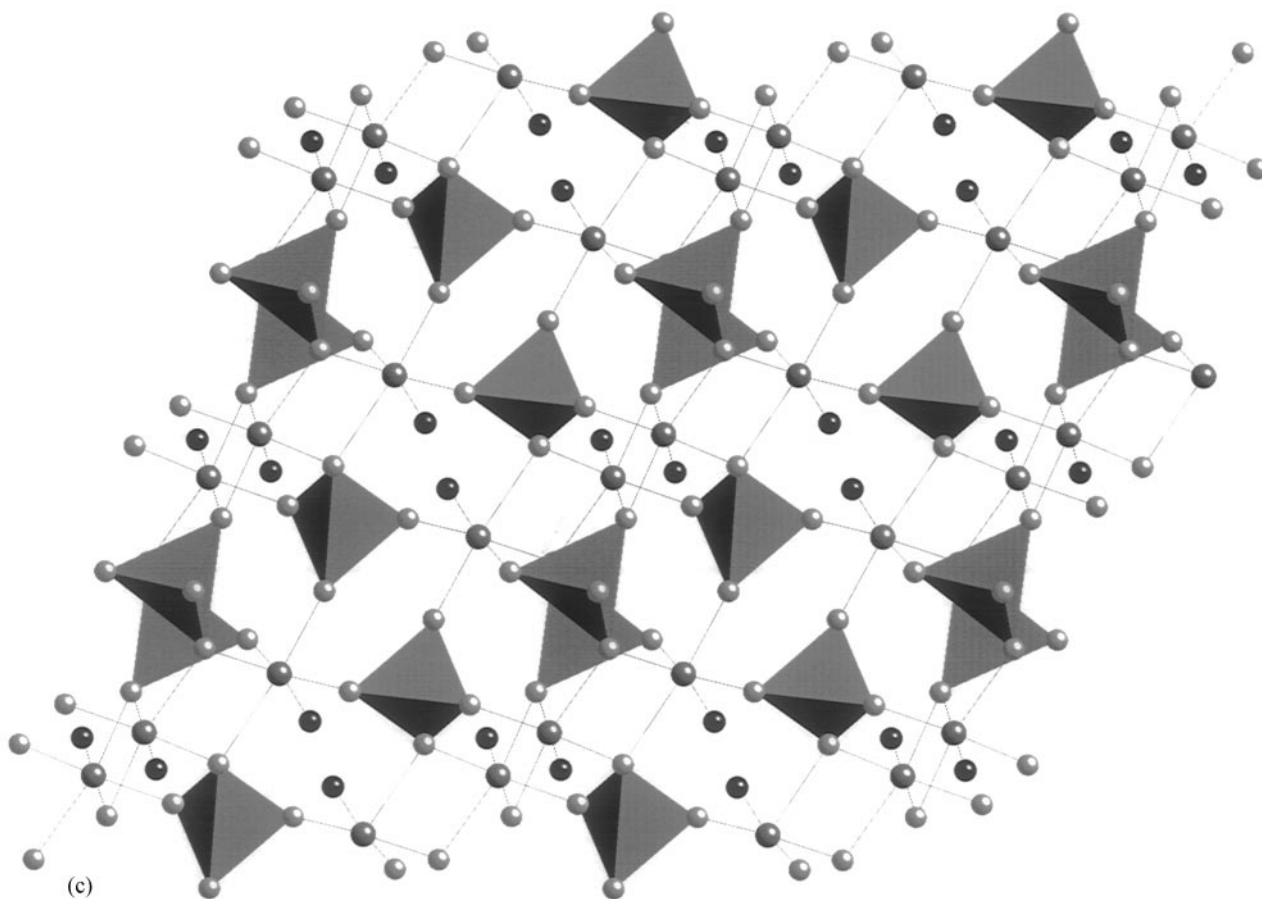


FIGURE 5—Continued

two binuclear  $\{\text{Cu}(\text{N}_2\text{O}_4)\text{Mo}(\text{NO}_5)\}$  units, producing a 28-membered ring. Furthermore, since only the Cu sites participate in ligation to two ligand units, these rings are offset by one polyhedral unit in successive layers, as shown in Fig. 4c.

The layer structure, shown in Fig. 5a, is quite distinct from those of MOXI-1 and MOXI-24 (Figs. 5b and 5c). The

structure may be described as  $\{\text{Mo}_4\text{O}_{13}\text{N}_2\}_n^{2n-}$  chains linked by  $\{\text{Cu}(\text{tpytrz})\}^{2+}$  units into a two-dimensional network of corner-sharing polyhedra. The molybdate chains are constructed from pairs of corner-sharing  $\{\text{MoNO}_5\}$  octahedra, linked through corner-sharing to  $\{\text{MoO}_4\}$  tetrahedra. The layer structure is distinguished by the presence

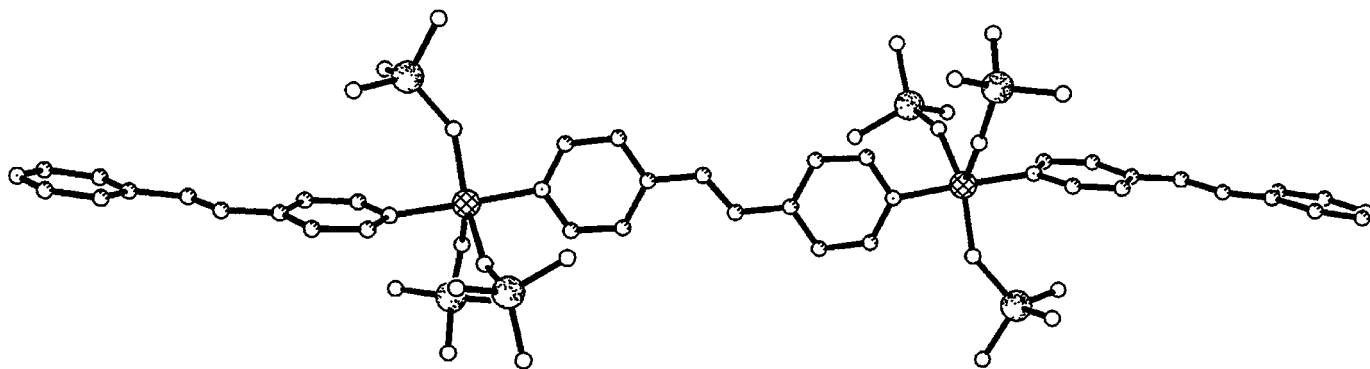


FIG. 6. The one-dimensional copper-(4,4'-dipyridylethene) chain of MOXI-1.

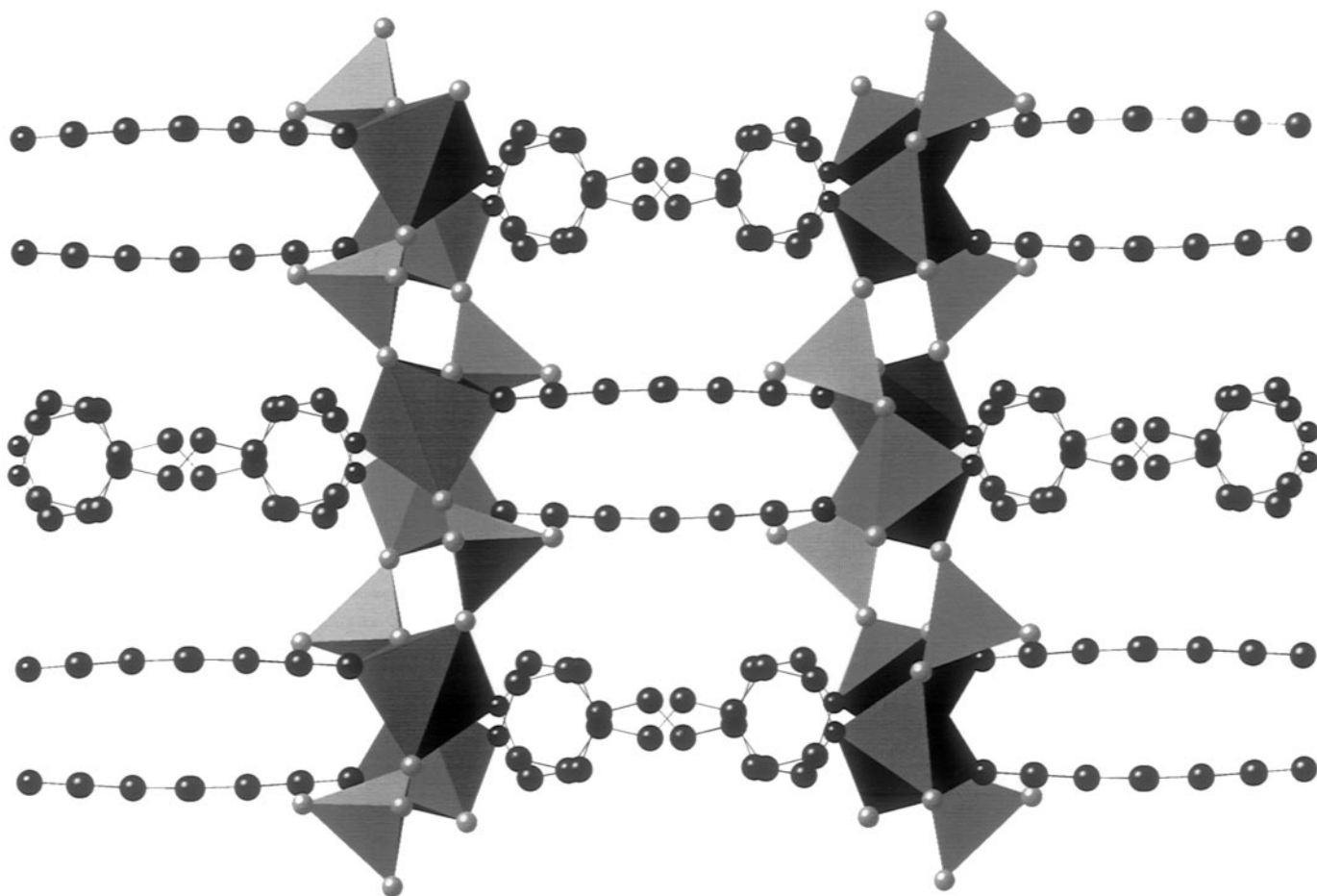


FIG. 7. A view parallel to the crystallographic  $a$  axis of the structure of **MOXI-1**.

of three annular substructures:  $\{\text{Cu}_2\text{Mo}_4\text{O}_6\}$ ,  $\{\text{Mo}_4\text{O}_4\}$ , and  $\{\text{Mo}_3\text{CuO}_3\}$  rings.

It is instructive to compare the details of the structure of **MOXI-37** to those of **MOXI-1** and **MOXI-24**. The fundamental building block of **MOXI-1** is shown in Fig. 6 and seen to consist of infinite  $\{\text{Cu}(4,4'\text{-bpe})\}_n^{2n-}$  chains, linked to  $\{\text{MoO}_4\}^{2-}$  tetrahedra. The Cu(II) coordination geometry is trigonal bipyramidal  $\{\text{CuN}_2\text{O}_3\}$ . The structure may be described as copper-bipyridylethene chains linked by molybdate tetrahedra into the layered structure of Fig. 7. As shown in Fig. 5b, the copper-molybdenum oxide layer consists of corner-sharing polyhedra, arranged such that there are no Mo-O-Mo or Cu-O-Cu pairings. Consequently, the fundamental layer motif is the  $\{\text{Cu}_3\text{Mo}_3\text{O}_6\}$  ring.

Figure 8 illustrates the layer structure of **MOXI-24**. In this case, the building block consists of Cu(II) sites from adjacent layers linked by the dipyridylamine ligand. The copper sites display  $\{\text{CuNO}_5\}$  octahedral geometry defined

by the nitrogen donor of the dpa ligand and oxygen atoms from five molybdate tetrahedra (Fig. 9a). A curious feature of the structure is the presence of tetranuclear copper clusters, constructed from edge-sharing copper octahedra, embedded within the copper-molybdate network, shown in Fig. 9b. Since the bpa-copper interactions do not find extension into Cu-ligand chains as in **MOXI-1**, the combination of tetranuclear copper subunits and bridging ligands generates an unusual layer registry, as shown in Fig. 9c. The two bpa ligands from adjacent copper sites of a cluster embedded in one layer link to copper sites from two clusters on the adjacent layer.

The network connectivity of **MOXI-24**, shown in Fig. 5c, consists of the tetranuclear clusters linked through corner-sharing  $\{\text{MoO}_4\}^{2-}$  tetrahedra into a  $\{\text{CuMoO}_4\}$  bimetallic layer. Each tetranuclear unit is linked to 10 molybdate polyhedra, while each molybdate unit bridges two copper sites of one tetranuclear unit and one site of an adjacent copper cluster.

## CONCLUSION

Hydrothermal synthesis provides a powerful tool for the introduction of nitrogen donor ligands into metal oxide structures. Consequently, organic components may be exploited in the modification of oxide microstructures. The structures of the title compound  $[\text{Cu}(\text{tpytrz})\text{Mo}_4\text{O}_{13}]$  and of the previously reported  $[\text{Cu}(\text{dpe})\text{MoO}_4]$  and  $[\text{Cu}(\text{bpa})_{0.5}\text{MoO}_4]$  exhibit the characteristic alternation of inorganic oxide networks and buttressing organic regions. However, the detailed connectivities within the networks are quite distinct for each structure. It is apparent that variations in ligand geometry produce profound changes in the oxide microstructures. While these observations demonstrate that the modification of oxide structures by organic components is readily achieved, predictability of structure remains elusive. It is noteworthy that these structures are primitive examples of hierarchically ordered materials which are nonequilibrium phases and thus path-dependent. Their intrinsic dynamic nature raises the problem of the essential complexity of these materials, which must set limits on the degree of synthetic predictability. However, from a more positive viewpoint, the rational design of materials requires not total predictability but rather a reciprocity of structure property relationships. Further insights into the architectural tailoring of such composite materials will require a significant expansion of the structural data base, such that as the products of empirical development are elucidated, the control of desired properties will evolve.

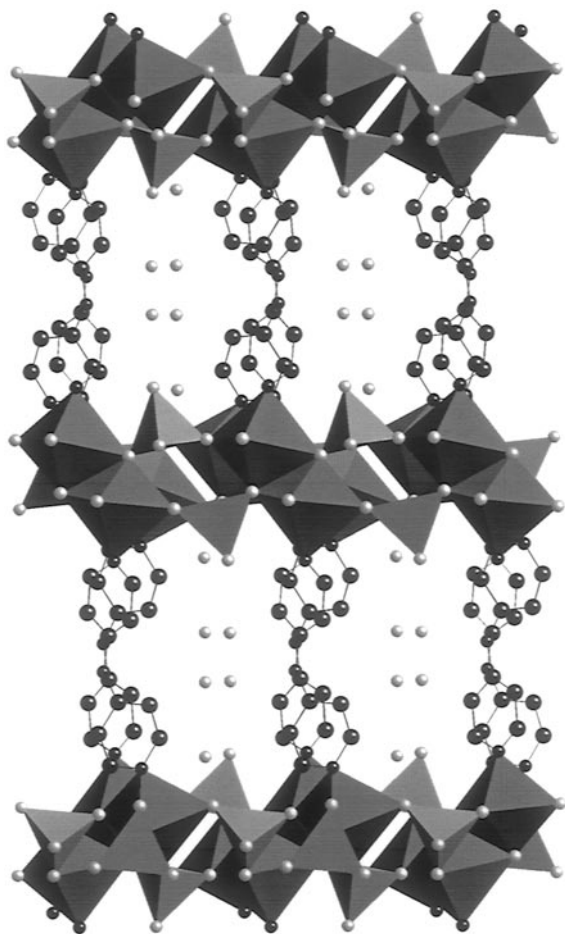


FIG. 8. A view parallel to the crystallographic  $a$  axis of the structure of MOXI-24.

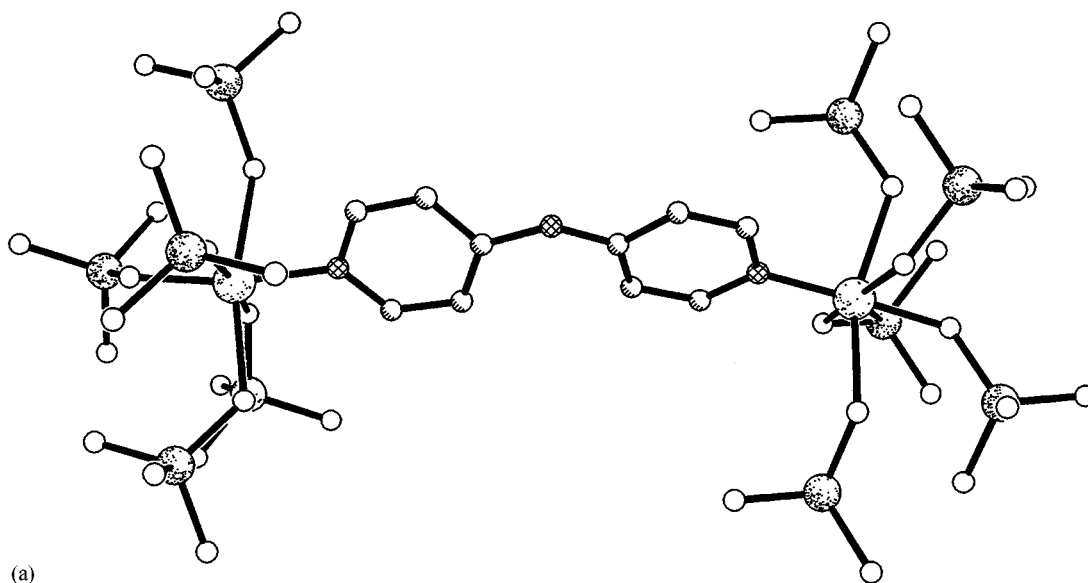
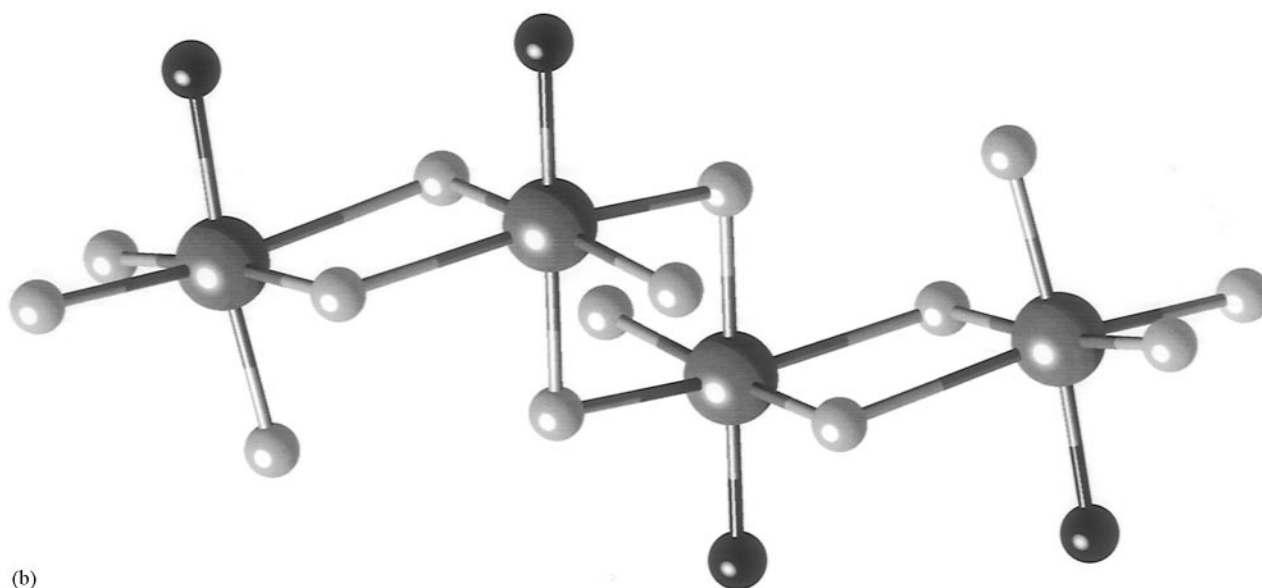
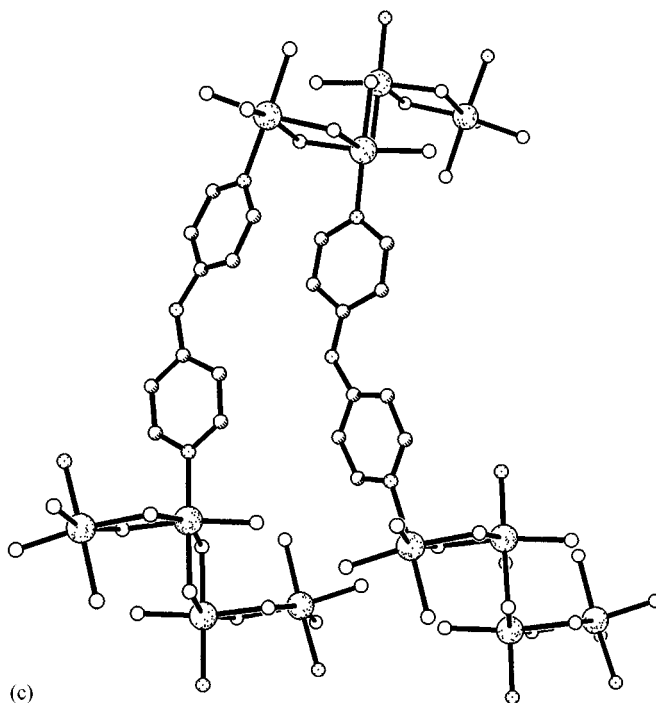


FIG. 9. (a) The linking of copper sites on adjacent layers by the bipyridylamine ligand. Each copper site is connected to five  $\{\text{MoO}_4\}$  tetrahedra. The Mo sites are heavily speckled, while the Cu centers are lightly speckled. Nitrogen atoms are cross-hatched and oxygen sites are open circles. (b) The tetranuclear copper cluster embedded in the  $\{\text{CuMoO}_4\}$  layers of MOXI-24. (c) The linking of copper clusters in adjacent layers through bpa ligands.



(b)



(c)

FIGURE 9—Continued

#### ACKNOWLEDGMENT

This work was supported by the National Science Foundation, Grant CHE9617232, and by a grant from the W. M. Keck Foundation.

#### REFERENCES

1. B. Cockayne and D. W. Jones (Eds.), "Modern Oxide Materials," Academic Press, New York, 1972.
2. W. Büchner, R. Schliebs, G. Winter, and K. H. Büchel, "Industrial Inorganic Chemistry," VCH, New York, 1989.
3. (a) J. A. Raleo, "Zeolite Chemistry and Catalysis," ACS Monograph 7, American Chemical Society, Washington, DC 1976; (b) Y. Murakami, A. Iijima, and J. W. Ward (Eds.), "New Developments in Zeolite Science," Elsevier, Amsterdam, 1986; (c) D. E. W. Vaughan, "Properties and Applications of Zeolites," (R. P. Townsend, Ed.), Chem. Soc. Special Publ. 33, p. 294, The Chemical Society, London, 1979; (d) P. B. Venuto, *Microporous Mater.* **2**, 297 (1994); (e) J. V. Smith, *Chem. Rev.*, **88**, 149 (1988); (f) M. L. Occelli and H. C. Robson, "Zeolite Synthesis," American Chemical Society, Washington, DC, 1989.

4. C. T. Kresge, M. E. Leonowicz, W. J. Roth, J. C. Vartuli, and J. S. Beck, *Nature* **359**, 710 (1992).
5. (a) R. C. Haushalter and L.A. Mundi, *Chem. Mater.* **4**, 31–48 (1992); (b) M. I. Khan, L. M. Meyer, R. C. Haushalter, C. L. Schweitzer, J. Zubieta, and J. L. Dye, *Chem. Mater.* **8**, 43 (1996).
6. “Crystal engineering” of metal–organic coordination 1D, 2D, and 3D solids has witness an explosive growth in the past decade. A particularly useful overview in terms of interpenetration is provided in S. R. Batten and R. Robson, *Angew. Chem. Int. Ed. Engl.* **37**, 1460 (1998), and references therein.
7. Some representative references from leading researchers in this vast field: (a) M. J. Zaworotko, *Chem. Soc. Rev.* **23**, 283 (1994); (b) H. Gudbjartson, K. Biradha, K. M. Poirier, and M. J. Zaworotko, *J. Am. Chem. Soc.* **121**, 2599 (1999); (c) B. F. Abrahams, P. A. Jackson, and R. Robson, *Angew. Chem. Int. Ed. Engl.* **37**, 2656 (1998); (d) L. Carlucci, G. Ciani, D. M. Proserpio, and A. Sironi, *Inorg. Chem.* **37**, 5941 (1998); (e) O. M. Yaghi, H. Li, C. Davis, D. Richardson, and T. L. Groy, *Acc. Chem. Res.* **31**, 474 (1998); (f) S. Lopez and S. W. Keller, *Inorg. Chem.* **38**, 1883 (1999); (g) M. Kondo, T. Okubo, A. Asami, S. Noro, T. Yoshitomi, S. Kitagawa, T. Ishii, H. Matsuzaka, and K. Seki, *Angew. Chem. Int. Ed. Engl.* **38**, 140 (1999); (h) D. M. L. Goodgame, D. A. Grachvogel, and D. J. Williams, *Angew. Chem. Int. Ed. Engl.* **38**, 153 (1999); (i) C. V. K. Sharma and R. D. Rogers, *Chem. Commun.* (1998); (j) M. Fujita, Y. J. Kwon, S. Washizu, and K. Ogura, *J. Am. Chem. Soc.* **116**, 1151 (1994); (k) M. A. Withersby, A. J. Blake, W. R. Champness, P. Hubberstey, W.-S. Li, and M. Schröder, *Angew. Chem. Int. Ed. Engl.* **37**, 2327 (1997); (l) A. J. Blake, S. J. Mill, P. Hubberstey, and W.-S. Li, *J. Chem. Soc. Dalton Trans.* 909 (1998); (m) J. S. Moore and S. Lee, *Chem. Ind. (London)* **14**, 556 (1994); (n) A. Mayr and J. Guo, *Inorg. Chem.* **38**, 921 (1999).
8. D. Hagrman, C. Zubieta, R. C. Haushalter, and J. Zubieta, *Angew. Chem. Int. Ed. Engl.* **36**, 873 (1997).
9. D. Hagrman, C. Sangregorio, C. J. O’Connor, and J. Zubieta, *J. Chem. Soc. Dalton Trans.*, 3707 (1999).
10. D. Hagrman, R.C. Haushalter, and J. Zubieta, *Chem. Mater.* **10**, 361 (1998).
11. D. Hagrman, C. J. Warren, R. C. Haushalter, and C. Seip, C. J. O’Connor, R. S. Rarig, Jr., K. M. Johnson, III, R. L. LaDuca, Jr., and J. Zubieta, *Chem. Mater.* **10**, 3294 (1998).
12. Siemens, “SMART Software Reference Manual,” Siemens Analytical X-ray Instruments, Inc., Madison, WI, 1994.
13. G. M. Sheldrick, “SADABS: Program for Empirical Absorption Corrections,” Univ. of Gottingen, Germany, 1996.
14. G. M. Sheldrick, “SHELXL96. Program for the Refinement of Crystal Structures,” Univ. of Gottingen, Germany, 1996.
15. A. Clearfield, *Prog. Inorg. Chem.* **47**, 371–510 (1998).